



ACT Project Number:  
**271498**

Project name:  
**ELEGANCY**

Project full title:  
**Enabling a Low-Carbon Economy via Hydrogen and CCS**

**ERA-Net ACT project**

Starting date: 2017-08-31  
Duration: 36 months

## **D2.1.4 Validation of Experimental Apparatus for Measurement of H<sub>2</sub> Solubility in Water/Brine**

**Date: 2018-11-30**

Organization name of lead participant for this deliverable:  
**Imperial College London**

<b>ACT ELEGANCY, Project No 271498, has received funding from DETEC (CH), BMWi (DE), RVO (NL), Gassnova (NO), BEIS (UK), Gassco, Equinor and Total, and is cofunded by the European Commission under the Horizon 2020 programme, ACT Grant Agreement No 691712.</b>		
<b>Dissemination Level</b>		
<b>PU</b>	Public	X
<b>CO</b>	Confidential, only for members of the consortium (including the Commission Services)	



<b>Deliverable number:</b>	D2.1.4
<b>Deliverable title:</b>	Validation of experimental apparatus for measurement of H <sub>2</sub> solubility in water/brine
<b>Work package:</b>	WP 2 CO <sub>2</sub> transport, injection and storage
<b>Lead participant:</b>	ICL

Authors		
Name	Organization	E-mail
Geraldine Torin-Ollarves	ICL	g.torin-ollarves@imperial.ac.uk
J P Martin Trusler*	ICL	m.trusler@imperial.ac.uk

\*Mark Lead Author with asterix

Keywords
Brine; Hydrogen; Solubility; Water

Abstract
<p>A new experimental apparatus has been designed, constructed and tested. This apparatus is to be used to measure the solubility of gases, such as H<sub>2</sub> and CO<sub>2</sub>, in water or brine at temperatures from ambient to 473 K and at pressures up to 70 MPa. The report details the design and construction of the equipment and presents the results of test measurements of the solubility of CO<sub>2</sub> in pure water. The test results are in close agreement with available models for CO<sub>2</sub> solubility in water that represent most of the literature data to within about 5%. These results confirm correct functioning of the experimental system.</p>



## TABLE OF CONTENTS

---

	Page
1 INTRODUCTION.....	1
2 DESIGN OF HIGH-PRESSURE GAS SOLUBILITY APPARATUS .....	2
2.1 Choice of experimental method.....	2
2.2 High-pressure view cell .....	3
2.3 Heater jacket and temperature-control system .....	4
2.4 Stirring system.....	4
2.5 Liquid-injection pump .....	5
2.6 Temperature and pressure sensors.....	5
2.7 Optical system .....	6
2.8 Integrated system.....	6
2.9 Safety system.....	7
3 VALIDATION OF THE HIGH-PRESSURE GAS-SOLUBILITY APPARATUS .....	8
3.1 Experimental protocol .....	8
3.2 Results for CO <sub>2</sub> solubility in H <sub>2</sub> O .....	9
4 CONCLUSIONS .....	11
5 APPENDICES .....	12
6 REFERENCES.....	18



## 1 INTRODUCTION

Reliable knowledge of the thermophysical properties of mixtures of CO<sub>2</sub> and numerous other substances are essential in designing the overall process of hydrogen production from fossil fuels with simultaneous capture, transportation and storage of CO<sub>2</sub>. Captured CO<sub>2</sub> is never pure, and, in this process, hydrogen is likely to be a significant impurity. This will affect the properties of the CO<sub>2</sub>-rich stream during pipeline transportation and influence the storage behavior once the fluid is injected into a storage reservoir [1]. In the case of aquifer storage, the key components of interest are CO<sub>2</sub>, impurities including H<sub>2</sub>, water, salts and the reservoir minerals with which these fluids are in contact. In the ELEGANCY project, one of the objectives is to improve the available thermodynamic-property models to encompass hydrogen and other impurities both under the conditions of pipeline transportation and under aquifer-storage reservoir conditions.

The specific objectives of Task 2.1 “Thermodynamic property model for CO<sub>2</sub>-brine” are to:

- Study the solubility behavior of CO<sub>2</sub> + H<sub>2</sub> in water and brines at reservoir conditions
- Develop a thermodynamic-property model to represent both this solubility behavior and the thermodynamic properties of the coexisting phases.

This report relates to first of these objectives and details the design, construction and validation of the experimental apparatus to be used in the measurement program.

## 2 DESIGN OF HIGH-PRESSURE GAS SOLUBILITY APPARATUS

### 2.1 Choice of experimental method

The experimental techniques for measuring vapor-liquid equilibria (VLE) at high pressures can be broadly categorized under the major headings of analytical and synthetic methods [2] and further sub-divided as illustrated in Fig. 2.1.

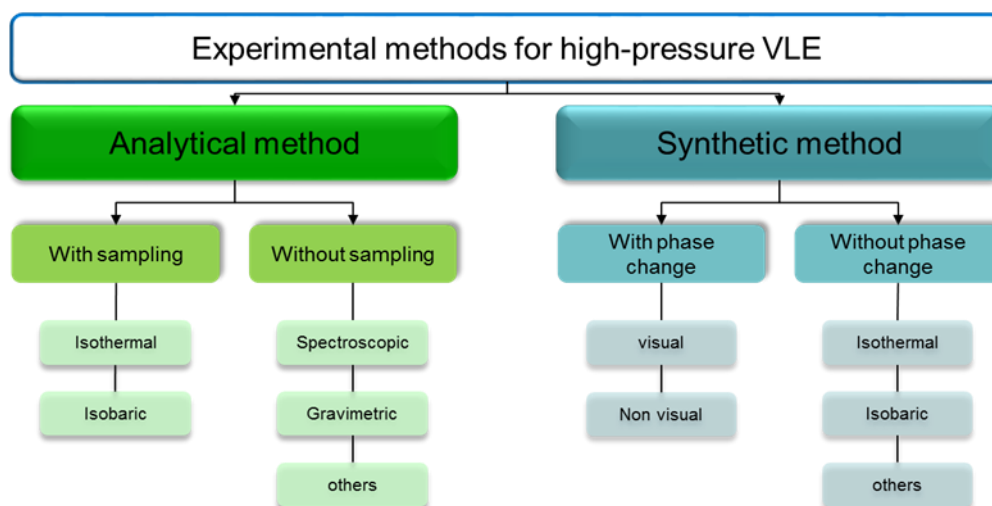


Figure 2.1: Classification of Experimental Methods [2].

In an analytical method, one brings the system containing two or more phases into a state of equilibrium and then measures the compositions of all coexisting phases by an appropriate technique. This approach provides very detailed information, especially for multi-component systems, but is generally quite complex and increasingly-difficult to implement at higher pressures. In the synthetic method, the overall composition of the system must be known and in the most common implementation (identified as ‘with phase change’ in Fig. 2.1) the system is caused to pass from a two-phase state to a single-phase state by adjusting the one of the state variables, *e.g.* volume. At the point where the system enters the single-phase region, one knows the composition of the phase, the temperature and the pressure. In VLE measurements on a binary system, measurements of both the bubble point and the dew point for the same overall composition can be obtained, resulting in the same information as yielded by the analytical method without the need for phase sampling or in-situ composition measurements. For multi-component systems, bubble and dew points can be obtained by coexisting-phase compositions are not determined.

In the present project, the main emphasis is on measurements of single-gas solubility (especially  $H_2$ ) in water or brine at high pressures. For this reason, the simpler synthetic approach is adopted, with phase change and visual observation.

In order to further simplify the method, a variable volume apparatus is not used; instead, the state of the system is scanned by continuous injection or withdrawal of the aqueous phase. A window is provided so that the transition from two-phase to single-phase states may be observed visually. In outline, the procedure is to fill a high-pressure view cell with a known amount of the gas under study and to inject the water or brine phase continuously with stirring until the last bubble of gas is seen to disappear. At that point, the temperature and pressure are recorded, and the amounts of gas and water/brine are known, the latter being obtained from the displacement of the injection pump. An important feature of the design, based on lessons learned in a previous project [3], is

that there must be no ‘dead’ volumes (*i.e.* trapped and/or unobservable) into which the gas can retreat as the liquid is injected. Gas in a trapped volume, such as the recess around a sealing ring, cannot mix effectively with the bulk of the liquid and, if unobserved, a false indication of the bubble point may result. Therefore, in the present design, the cell has just a single window, around which some dead volume is essentially unavoidable, and its orientation ensures that the gas is pushed towards the closed end of the cell as liquid is injected. In this way, the gas has nowhere to go except to dissolve in the liquid. A second important feature of the design is that the view cell has been fabricated from materials that are resistant to corrosion in concentrated brines: titanium alloy, sapphire and perfluoro elastomer.

## 2.2 High-pressure view cell

The cell view, which is the heart of the system, has been designed for operation at pressures up to 70 MPa with temperatures from ambient to 473 K. Figure 2.2 provides an overview of the view cell. The monobloc body was fabricated from titanium grade 5 alloy. It was provided with two high-pressure fluid ports and closed at one end by a large sapphire window held in place by a threaded retaining ring and sealed by a circumferential o-ring. A hole bored in the wall of the vessel, parallel to the cylindrical axis, is provided to permit installation of a platinum resistance thermometer (PRT) probe for measurement of the cell temperature.

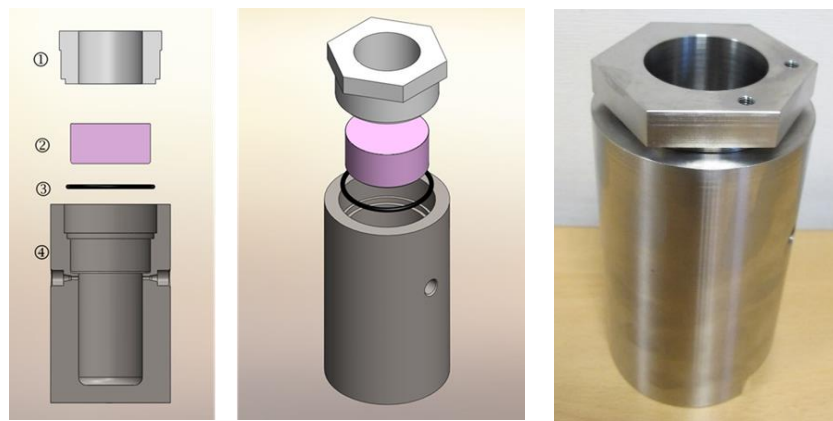


Figure 2.2: Left: exploded cross-sectional of the cell showing: (1) retaining ring; (2) sapphire window; (3) o-ring; and (4) cell body. Middle: exploded perspective view. Right: photograph of the assembled view cell.

The mechanical design of the vessel was based on conservative principles whereby no part of the metal cell would be subjected to more than  $\frac{2}{3}$  of the yields strength or  $\frac{1}{4}$  of the ultimate tensile strength. The window thickness was chosen such that there was a safety factor of 4 relative to an apparent elastic limit specified by the manufacturer.

Appendix A shows the full technical drawings while Appendix B summarizes the mechanical design calculations.

Following construction, the cell was subjected to a hydrostatic pressure tested at 125 MPa without the window in place; this pressure based on 1.5 x the maximum working pressure with an additional margin of about 19% to reflect the decline in the yield strength between the test temperature and the maximum service temperature. The pressure test certificate is included as Appendix C. A second test with the window in place was carried out at 1.5 x the maximum

working pressure, *i.e.* 105 MPa, with the sapphire window in place. In both cases, the vessel passed and there was no evidence of leakage.

### 2.3 Heater jacket and temperature-control system

In order to maintain constant temperature of the vessel and its contents, an aluminum heater jacket was designed as shown in Fig. 2.3. This comprised four sections that could be assembled around the view cell, enclosing all of it except for the window area. Technical drawings are provided in Appendix A. Heating was provided by a set of four electric cartridge heaters, and two axial holes were bored to accommodate additional PRT probes: one for use by the temperature controller and a second for use in the safety system. When assembled, the outer surface of the heating jacket was insulated with a thick layer of silicone-rubber sponge.



Figure 2.3: From left to right: photographs of the heating jacket components; heating jacket components with view cell; electric cartridge heater; and process controller.

Temperature control was provided by a Eurotherm model 2216e process controller operating with the PRT temperature sensors, 230 Vac solid-state relay output and the electric cartridge heaters.

### 2.4 Stirring system

Good mixing is essential to promote the attainment of an equilibrium state in the vessel. In the new cell, stirring was provided by a stirrer bar coupled magnetically to an external permanent magnet which was rotated by a variable-speed motor. The magnet assembly comprised two samarium-cobalt magnets (20 mm x 35 mm x 40 mm) yoked together by a steel plate (10 mm x 40 mm x 70 mm) as shown in Fig. 2.4. The steel plate was provided with a central screw hole to allow it to be attached to the end of a shaft coupled to the motor, also shown in Fig. 2.4.



Figure 2.4: Left, permanent magnet assembly; right, motor and speed controller.

The induction motor (Panasonic model M61X6GV4GGA) and speed controller (Panasonic model DVUS990GE) permitted operation in the speed range from 90 to 1400 rpm. Stirring was typically operated at about 300 rpm.

The stirring system was arranged such that the axis of rotation was concentric with the view cell with the poles of the magnet located just outside the closed end of the vessel. The coupling between the stirrer bar and the magnet was sufficiently strong to keep the stirrer bar centered on the closed end of the view cell whatever the orientation of the vessel.

## 2.5 Liquid-injection pump

Water or brine was injected from an ISCO model 100DM high-pressure syringe pump with Hastelloy wetted parts, 103 mL capacity and 70 MPa maximum working pressure. The pump, shown in Fig. 2.5, was digitally controlled and could be operated in constant flow rate, constant pressure or ramped volume or pressure modes. During normal operation, the pump was operated in a sequence of pressure ramps during which the pressure was changed linearly with time from an initial value to a final value in a programmed period of time. The pump module was fitted with an internal pressure sensor which provided a control signal to the controller during constant or ramped pressures operations.

The mass of solvent (water or brine) delivered by the pump is, in practice, calculated from the swept volume and knowledge of the density of the solvent as a function of temperature and pressure. In order to ensure a constant temperature, the pump cylinder was fitted with a thermostatic jacket through which water was circulated from a thermostatically-controlled circulator. The piston was sealed by means of a PTFE-composite lip seal as shown in Fig 2.5.



Figure 2.5: High pressure syringe pump. Left, pump and control modules; Middle, thermostatic jacket fitted to pump cylinder; Right, piston sealing ring.

## 2.6 Temperature and pressure sensors

Two pressure sensors were installed in the system at any one time: one to measure the initial (low) gas filling pressure and the second to monitor the pressure during the process of liquid injection up to the bubble point. These pressure sensors were Keller series 35 X. The gas pressure sensor used in initial validation had a range of (0 to 3) MPa; this could be interchanged for (0 to 1) MPa range for use when lower filling pressures were required. The second pressure sensor had a range

of (0 to 70) MPa. All sensors were characterized by a relative uncertainty of 0.05% of reading. Pressure data were logged digitally and also displayed on a local display module. Fig. 2.5 shows the pressure sensors and display.



Figure 2.5. Left, Keller 35X pressure sensor; Middle, Keller pressure display module; Right, platinum resistance thermometer.

Platinum resistance thermometer probes were purchased from TC Direct with the following dimensions: probe length 100 mm; probe diameter 3.0 mm. These thermometers were calibrated in our laboratory; the sensor used to measure the cell temperature had an uncertainty after calibration of  $< 0.05$  K. Resistances were measured with an Agilent data acquisition unit, model 34970A.

## 2.7 Optical system

In order to observe the interior of the vessel and to detect small bubbles, a CCD camera (Ealing Optics model EO-0413C) fitted with a zoom lens (Computar model MLH-10X Macro lens 13-130mm 1/2" Manual Zoom C-mount) and an LED 'halo' lighting ring (Close-Ups model 60 LED Ring Light) was used. The camera and view cell were mounted in coaxial alignment on a flat, rigid plate. Digitized CCD images were captured by the control computer and saved, with time stamps, for later analysis.

## 2.8 Integrated system

The main components, except for the ISCO pump, were mounted on a frame. The plate supporting the view cell and optical system was mounted on a rotatable axis so that the vessel could be orientated with its axis at inclinations to the horizontal of between  $-90^\circ$  and  $+90^\circ$ . Tubing connections were completed in flexible 1/16" o.d. Hastelloy tubing which were able to accommodate this movement. Fig. 2.6 shows the integrated assembly.





### 3 VALIDATION OF THE HIGH-PRESSURE GAS-SOLUBILITY APPARATUS

The apparatus has been validated by means of measuring the solubility of CO<sub>2</sub> in pure water at several temperatures and pressures and comparing the results with available models. This is a sound validation strategy as the solubility of CO<sub>2</sub> in pure water is well studied and known to within about 5% under the conditions investigated.

#### 3.1 Experimental protocol

A detailed protocol was developed. Starting with a clean and evacuated system, the protocol was as follows (with reference to Fig 2.7):

1. Fill the liquid bottle with pure water.
2. Set the desired operating temperature.
3. Close V2, open V1 and allow water to flow into the evacuated pump.
4. Close V1, raise pressure in the pump and purge to waste through V2 and V3. Refill the pump through V1.
5. Isolate the outlet of the cell at V6 and isolate the liquid inlet at V3.
6. Slowly open V4 and admit gas until a pre-determined filling pressure is reached.
7. Allow the system to reach equilibrium and record the temperature and pressure of the gas.
8. Turn on the stirring mechanism, open valve V2 and V3, and start to transfer liquid into the cell.
9. When the cell is partially filled with liquid and the pressure is above the expected bubble pressure, stop the transfer of liquid and continue stirring until the gas is completely dissolved in the liquid.
10. Once the gas is completely dissolved and the pressure and temperature are stable, start a pressure ramp in which the pressure is decreased slowly at a rate of about 1.80 MPa/h until a pressure below the expected bubble point is reached and two phases are clearly observed.
11. Determine the bubble point visual observation and/or a change in slope of a graph of the pump volume vs. time at constant pressure ramping rate or the pump volume vs. pressure.
12. At the conclusion of the measurement, discharge the cell contents to waste through V6. The cell temperature may also be elevated above the boiling point of water to help empty the cell.
13. Finally, evacuate the system, through V6 and V8.
14. If, during steps 12 and 13, the syringe pump is not emptied then, in a subsequent experiment, steps 3 and 4 are unnecessary.

When the bubble point is entirely unknown, it may be necessary to carry out the procedure two or more times, initially with a rapid pressure ramp in step 10 to allow quick but approximate location of the bubble point and then more slowly to ensure a precise determination. This protocol will require minor modification when water is replaced by brine.

### 3.2 Results for CO<sub>2</sub> solubility in H<sub>2</sub>O

Validation measurements were made for CO<sub>2</sub> solubility in pure water. Measurements were made at temperatures of 323.15 K, 373.15 K and 423.15 K. At the middle temperature, three different filling pressures were used, resulting in three bubble-point determinations, while at the other two temperatures just a single measurement was made. Fig. 3.1 shows examples of the measured data close to the bubble point, together with the graphical construction used to determine the precise bubble-point pressure  $p_b$ .

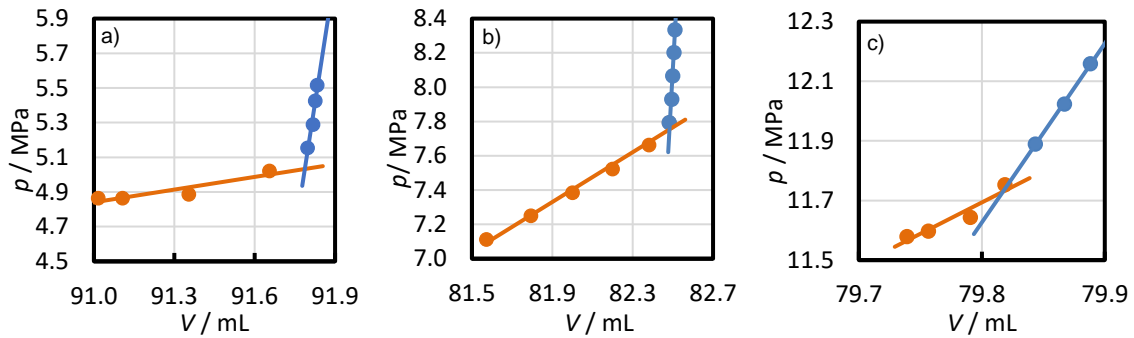


Figure 3.1: Pressure-volume diagrams for determination of the bubble point of CO<sub>2</sub> + H<sub>2</sub>O mixtures where  $V$  is the volume of water, measured at the syringe pump, injected into the cell. Symbols: ●; two-phase region; ●, single-phase region. Lines represent linear regressions used to determine the bubble point by intersection. From left to right: a)  $T = 323.15$  K, b)  $T = 373.15$  K, and c)  $T = 423.15$  K.

The results of the five bubble-point determinations are given in Table 3.1 where the experimental results are an average of three runs for each temperature and initial filling pressure. These values are plotted in Fig. 3.2 in comparison with two leading models. The models considered here are those of Spycher and Pruess [4] and Duan et al. [5]. There is close agreement between the both models and the experimental data measured in this project; this provides the required validation of the experimental method. A detailed analysis of the experimental uncertainty has not yet been carried out but it is likely to be similar to that found in earlier work [3]: 0.00015 for mole fraction and <0.15 MPa for bubble pressure, both at 95% confidence. The uncertainty of the models is stated to be around 5% of  $p_b$  at given  $x_{\text{CO}_2}$  and, considering this tolerance, the new data can be considered in excellent agreement with the models.

Table 3.1. Experimental results for CO<sub>2</sub> solubility in water: temperature  $T$ , initial CO<sub>2</sub> filling pressure  $p_{\text{fill}}$ , bubble pressure  $p_b$  determined by both PVT measurements and visual observation, and the mole fraction  $x$  of dissolved CO<sub>2</sub>.

$T/\text{K}$	$p_{\text{fill}}/\text{MPa}$	$p_b/\text{MPa}$ *		$x$
		PVT	Visual	
323.15	1.81	5.03	5.16	0.0137
373.15	1.09	4.13	4.30	0.0062
373.15	1.82	7.75	7.74	0.0120
373.15	2.56	13.38	13.32	0.0167
423.15	2.40	11.77	11.78	0.0144

\*Average of three runs

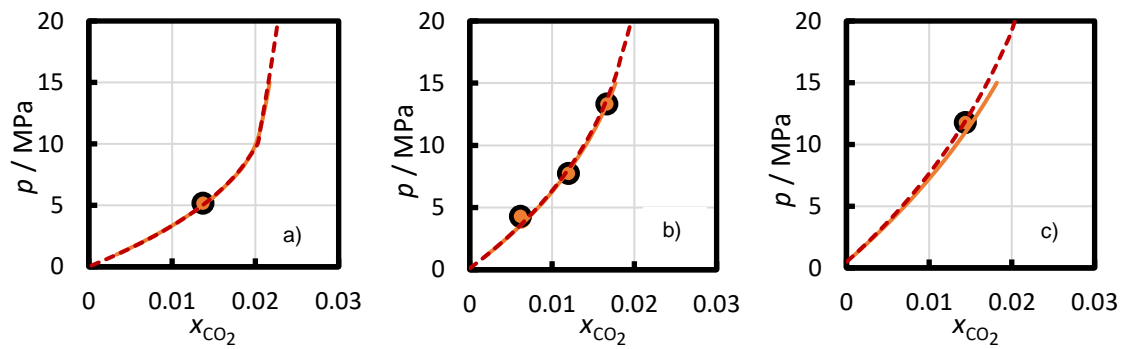


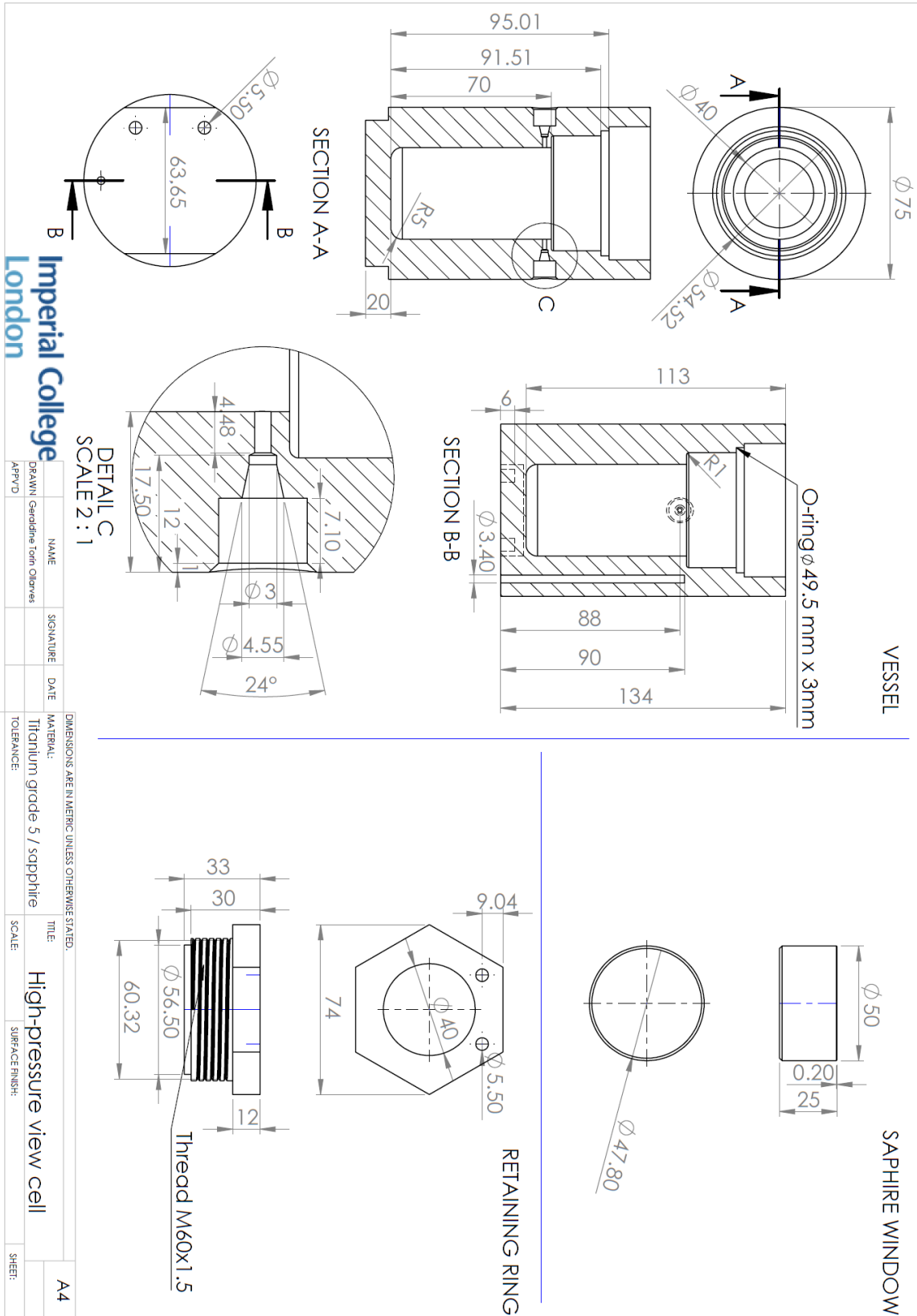
Figure 3.2: Results for  $\text{CO}_2$  solubility in water and comparison with the models of Sphycher & Pruess (solid curves) and Duan et al. (dashed curves). Symbols: ●, determined from PVT data, ○ determined by visual observation. From left to right: a)  $T = 323.15$  K, b)  $T = 373.15$  K, and c)  $T = 423.15$  K.

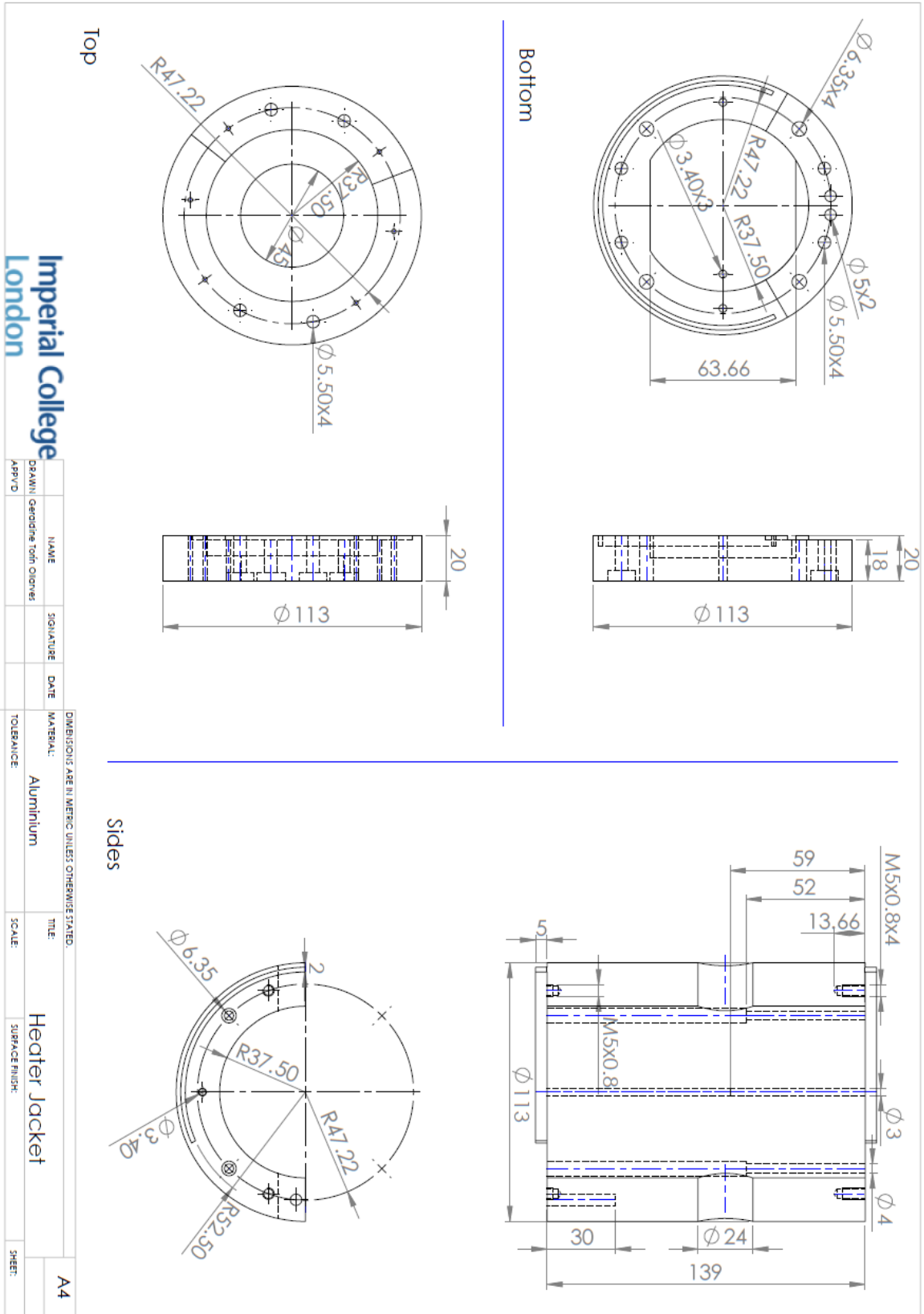
## 4 CONCLUSIONS

At this stage in the project, the experimental apparatus is fully developed and validated. The results presented in this report demonstrate that the apparatus, with the experimental protocol followed, yields reliable results. The next steps will be to carry out a few test measurements on N<sub>2</sub> solubility in water, followed by a program of measurements of H<sub>2</sub> solubility in water and brine.

5 APPENDICES

A APPENDIX A: ENGINEERING DRAWINGS





## B APPENDIX B: MECHANICAL DESIGN SUMMARY

The mechanical design of the view cell body and window closure are detailed below in Table B.1

Table B.1: Mechanical design of the view cell. Highlighted cells are user inputs.

<b>PED Category</b>			
Fluid State	1	Gas or (Gas + Liquid)	
Fluid Group	1	Hazardous fluids	
$p_w/\text{MPa} =$	70	Maximum working pressure	
$T_w/^\circ\text{C} =$	200	Maximum working temperature	
$T_t/^\circ\text{C} =$	25	Hydrostatic test temperature	
$p_{\text{test}}/\text{MPa} =$	125	Hydrostatic test pressure (without window)	
PED Category	SEP	Sound Engineering Practice	
<b>Body material:</b>	<b>Ti Grade 5</b>		
$\sigma_{y,w}/(\text{N}/\text{mm}^2) =$	690	Yield stress at maximum service temperature	
$\sigma_{u,w}/(\text{N}/\text{mm}^2) =$	798	Ultimate tensile stress at maximum service temperature	
$\sigma_{y,t}/(\text{N}/\text{mm}^2) =$	823	Yield stress at test temperature	
M =	4	Shear stress safety factor	
$\tau_{\text{max}}/(\text{N}/\text{mm}^2) =$	86	Maximum shear stress, including safety factor	
<b>Window material:</b>	<b>Sapphire</b>		
$F_a/(\text{N}/\text{mm}^2) =$	250.0	Apparent elastic limit	
			<b>Pass/Fail</b>
<b>Cylinder</b>			<b>Pass</b>
ID/mm =	40.0	ID of cylinder	
OD/mm =	75.0	OD of cylinder	
L/mm =	70.0	Internal length	
V/mL =	88.0	Max. internal volume	
K =	1.88	Ratio between OD and ID of cylinder	
$\frac{2}{3}p_y/\text{MPa} =$	164.6	Yield stress criterion: $p_w \leq \frac{2}{3}p_y$	
$\frac{1}{4}p_u/\text{MPa} =$	121.4	Burst pressure criterion: $p_w \leq \frac{1}{4}p_u$	
<b>Base</b>			<b>Pass</b>
t/mm =	20.0	Thickness of base	
Y =	1.43	Minimum cylindrical wall thickness ratio	
$t_b/\text{mm} =$	17.0	Minimum base thickness (corner stress criterion)	
$(4t\tau_{\text{max}}/D)/\text{MPa} =$	172.5	Shear stress criterion on base	
<b>Retaining ring and window</b>			<b>Pass</b>
D/mm =	50	Window diameter (= effective sealing diameter)	
t/mm =	25	Window thickness	
$D_1/\text{mm} =$	40	Ring ID (= unsupported diameter of window)	
$D_t/\text{mm} =$	60	Major thread diameter	
$L_t/\text{mm} =$	19	Length of engaged thread	
$(9F_a/8)(t/D_1)^2/\text{MPa} =$	109.9	Window stress criterion (unclamped @ $1.5p_w$ )	
$(4D_tL_t\tau_{\text{max}}/D^2)/\text{MPa} =$	157.3	Thread shear stress criterion	

Figure B.1 shows the definitions of the dimensions  $L_t$ ,  $D_t$ ,  $D_1$  and  $t$  relating to the window and retaining ring. The design of the window includes a safety factor of 4 on the thickness  $t$  and treats the window as an unclamped disc with an apparent elastic limit (specified by the window supplier) of 250 MPa. A thin PEEK washer is used between the retaining ring and the window to prevent metal-to-sapphire contact and help to spread the load evenly around the perimeter of the window.

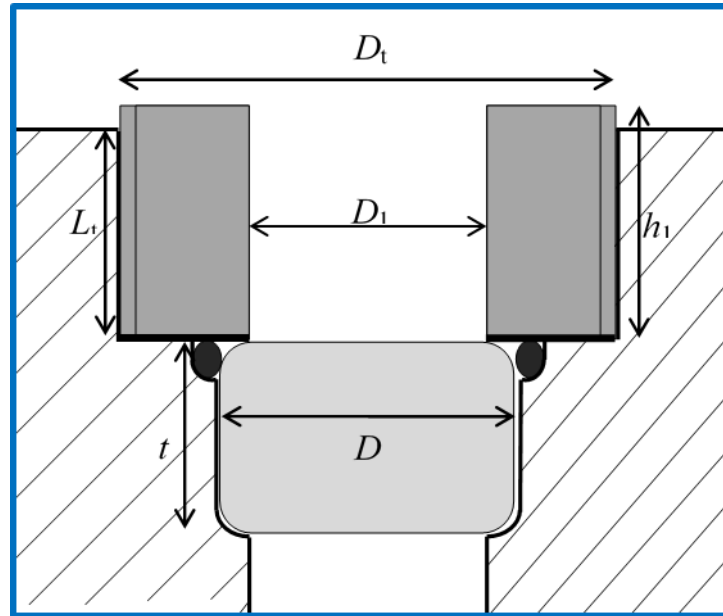
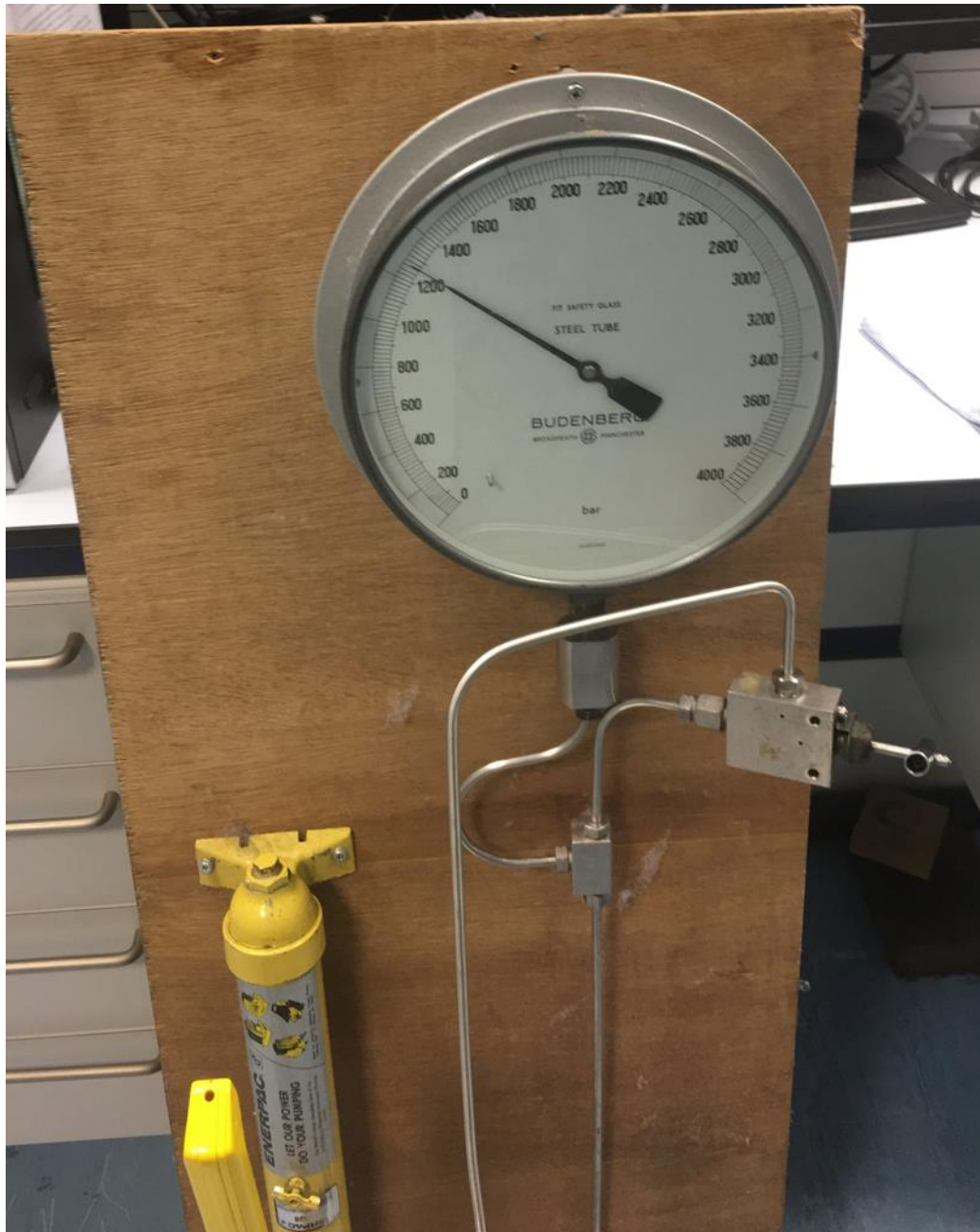


Figure B.1: Definitions of key dimensions of the window and retaining ring.

## C APPENDIX C: PRESSURE TEST CERTIFICATE

### Pressure Test Certificate

<b>Description:</b>		
<b>Material:</b> Titanium grade 5		
<b>Overall external dimensions:</b> H = 134 mm; D = 75 mm		
<b>Inner dimensions:</b> H = 70 mm; D = 40 mm		
<b>Manufacturer:</b> Chemical Engineering workshop, Imperial College London.		
<b>Year of construction:</b> 2018		
<b>Specifications</b>		
Operating Pressure <b>OP Min./Max. (bar)</b>	0	700
Operating Temperature <b>OT Min./Max. (°C)</b>	0	200
Capacity <b>V (litre)</b>	0.09	
Test Pressure <b>PT (bar)</b>	1250	
<b>Specific Tests</b>		
	<b>Pressure (bar)</b>	<b>Duration at test pressure (min)</b>
Leak Test Medium: water	150	5
Proof Pressure Test Medium: water	1250	15
Remarks	No leakage observed. Photos appended.	
<b>Test Result:</b>		
The vessel conforms to the requirements under sound engineering practice.		
Tested by: Dr G A Torin Ollarves		Witnessed by: Prof. J P M Trusler
<i>Geraldine Torin Ollarves</i>		<i>J.P.M. Trusler</i>
Date: 12 July 2018		



*Figure C.1: Photograph of the hydraulic pressure generator set unit showing the test pressure reading of approximately 1250 bar = 125 MPa. The outlet of the hydraulic pump was connected to the vessel under test.*

## 6 REFERENCES

- [1] J.P.M. Trusler, Annual Review of Chemical and Biomolecular Engineering 8 (2017) 381-402.
- [2] R. Dohrn, S. Peper, J.M.S. Fonseca, Fluid Phase Equilib. 288 (2010) 1-54.
- [3] D. Tong, J.P.M. Trusler, D. Vega-Maza, J. Chem. Eng. Data 58 (2013) 2116-2124.
- [4] N. Spycher, K. Pruess, Transport Porous Med. 82 (2010) 173-196.
- [5] Z. Duan, R. Sun, C. Zhu, I.M. Chou, Mar. Chem. 98 (2006) 131-139.